RSC Advances

PAPER

View Article Online
View Journal | View Issue

Cite this: *RSC Adv.*, 2015, **5**, 33999

One-step synthesis of carboxyl-functionalized rare-earth fluoride nanoparticles for cell imaging and drug delivery†

Zhiyang Zhang,[a] Xiaoyan Ma,[a] Zhirong Geng,*[a] Kuaibing Wang[ab] and Zhilin Wang*[a]

Received 4th February 2015
Accepted 3rd April 2015

DOI: 10.1039/c5ra02217g

www.rsc.org/advances

Rare-earth doped UCNPs with a carboxyl coating on the surface have been widely used in many fields of biology, however, the modification of nanoparticles with a carboxyl polymer group is relatively complicated, and thus, fabricating carboxyl polymer-coated UCNPs using a simple method is significant. Herein, we synthesized carboxyl polymer-coated $NaYF_4$:Yb^{3+}/Tm^{3+} nanoparticles through a hydrothermal route during which methacrylic acid polymerized and bound to the surface of the nanoparticles. Dependence of structure and morphology on the dosage of NaOH was investigated. The polymerization degree of poly(methacrylic acid) and the amount of capping carboxyl group influenced by the dosage of NaOH were also studied. Other carboxyl-functionalized rare-earth fluorides could be obtained by using this method, the mechanism for which was also investigated. Thus, this method was universal for the carboxyl capping of rare-earth doped fluoride nano-materials, and also provided a new approach for carboxylic functionalization of nanoparticles. *cis*-Dichlorodiammineplatinum(II) (*cis*platin, CDDP)-loaded $NaYF_4$:Yb^{3+}/Tm^{3+} nanoparticles ($NaYF_4$–CDDP) were characterized by transmission electron microscopy, energy-dispersive X-ray spectroscopy and X-ray photoelectron spectroscopy, and CDDP was loaded in the form of Pt–O bonds. Upconversion luminescence images revealed the time course of intracellular CDDP delivery by $NaYF_4$–CDDP. Compared with CDDP alone, the $NaYF_4$–CDDP composite exerted cytotoxic effects on HeLa and MCF-7 cancer cell lines depending more on time and more slowly due to time-dependent cellular uptake and drug release. Non-loaded $NaYF_4$:Yb^{3+}/Tm^{3+} nanoparticles were also eligible for upconversion luminescence cell imaging. Therefore, the as-prepared $NaYF_4$:Yb^{3+}/Tm^{3+} nanoparticles allow simultaneous cell imaging and drug delivery as promising anti-cancer theranostic agents.

Introduction

Rare-earth doped nanoparticles have been widely studied due to their unique luminescence properties originating from f–f electronic transitions among the 4f electrons of rare-earth ions. Downconversion and upconversion luminescence can be observed when different rare-earth ions are doped.[1–4] Rare-earth doped nanoparticles have many advantages. The luminescence property of rare-earth doped nanoparticles is not so dependent on the particle sizes as other luminescence nanomaterials such as Au, Ag and carbon.[5–7] And compared with conventional luminescent probes such as organic fluorescent dyes and quantum dots,[8–10] rare-earth doped nanophosphors exhibit higher photostability, chemical stability and lower biotoxicity.[11] Especially, the upconversion process, which converts near-infrared radiation to UV or visible luminescence through multi-photon absorption,[11,12] is advantageous in weak auto-fluorescence background, light-penetration depth in tissues and minimum photodamage to living organisms,[13–15] thus in favor of biological uses. Though multi-photon absorption process can occur in some Au and Ag nanoparticles, the pulse laser for excitation is more costly compared to continuous wave laser used for excitation of rare-earth doped upconversion nanoparticles (UCNPs).[16,17] Besides, some Ag and carbon containing nanomaterials express some biotoxicity.[18–21] Thus, UCNPs with superior luminescent property and biocompatibility are widely used in the field of biology.

Carboxyl group is usually introduced onto the surface of UCNPs to improve their aqueous solubility and bind other molecular for multifunctional bioapplications both *in vitro* and *in vivo*, such as bioprobe, bioimaging and drug delivery, *etc.*[22–26]

[a]*State Key Laboratory of Coordination Chemistry, School of Chemistry and Chemical Engineering, Collaborative Innovation Center of Advanced Microstructures, Nanjing University, Nanjing 210093, P. R. China. E-mail: wangzl@nju.edu.cn; gengzr@nju.edu.cn; Fax: +86-25-83317761; Tel: +86-25-83686082*

[b]*School of Science, Nanjing Agricultural University, Nanjing 210095, P. R. China*

† Electronic supplementary information (ESI) available: ESI-MS results of solute in supernatant from production prepared with different amounts of NaOH, MAA monomer, and solute in supernatant with and without rare-earth ions, TEM image of UCNPs–CDDP composite, ESI-MS result of solute in supernatant from reaction system for $NaGdF_4$:Yb^{3+}/Er^{3+} preparation, IR spectrum of $NaGdF_4$:Yb^{3+}/Er^{3+}, TEM image of $NaGdF_4$:Yb^{3+}/Er^{3+}. See DOI: 10.1039/c5ra02217g

Carboxyl polymers not only produce abundant carboxyl, compared to small carboxyl molecular, they can also provide hydrophily and protect luminescence core from nonradiative relaxation of water more effectively.[27] Thus carboxyl polymers become common method for carboxyl supplying, and many methods such as direct synthesis and surface functionalization have been developed to cap nanoparticles with carboxyl polymer group. Carboxyl polymers, such as sodium polyacrylate and polyacrylic acid, have been used to cap UCNPs through a one-step solvothermal route, but the reaction temperature requirement is relatively high.[28–31] For hydrophobic UCNPs, generally, there are three strategies to provide a carboxyl polymer-functionalized surface,[4,32] such as ligand exchange,[27,33] ligand attraction[34,35] and *in situ* surface polymerization.[36,37] These methods have been proved feasible, but the process for surface functionalization is usually more than two steps which is laborious.[32] Therefore, it is of great significance to develop a simple and flexible approach to prepare UCNPs coated with carboxyl polymer ligands. Inspired by the *in situ* polymerization method, herein we developed a facile strategy that prepared carboxyl polymer coated $NaYF_4$:Yb^{3+}/Tm^{3+} nanoparticles in one step. In the synthesis process, UCNPs crystallized and carboxyl polymer formed through polymerization of methacrylic acid (MAA) simultaneously, not only avoiding the complicated modification process, also reducing the reaction temperature. To the best of our knowledge, this method for preparation of carboxyl group functionalized nanoparticles has not been reported hitherto.

In this study, carboxyl polymer-coated $NaYF_4$:Yb^{3+}/Tm^{3+} nanoparticles were prepared base on a hydrothermal route during which MAA polymerized and bound to the surface of $NaYF_4$:Yb^{3+}/Tm^{3+} nanoparticles. Polymerization degree of poly-(methacrylic acid) (PMAA), amount of carboxyl and crystal phase of $NaYF_4$:Yb^{3+}/Tm^{3+} nanoparticles were adjusted by changing the dosage of NaOH. Furthermore, a series of carboxyl polymer-functionalized rare-earth fluorides could be obtained by using this method, and the formation process was investigated by changing the hydrothermal time. Accordingly, this method was universal for the carboxyl capping of rare-earth doped fluorides nano-materials. In order to evaluate the bioapplication of as prepared $NaYF_4$:Yb^{3+}/Tm^{3+} nanoparticles, CDDP was tethered onto their surface ($NaYF_4$–CDDP) through carboxyl group to establish a drug delivery system. Cellular uptake process was monitored by detecting the upconversion luminescence of $NaYF_4$:Yb^{3+}/Tm^{3+} nanoparticles. MTT assay showed that the as-prepared $NaYF_4$–CDDP composite was cytotoxic, thus confirming that the as-established drug delivery system was effective. Being luminescent, biocompatible and hydrophilic, the $NaYF_4$:Yb^{3+}/Tm^{3+} nanoparticles were particularly suitable for cell imaging.

Experimental

Materials

$Y(NO_3)_3 \cdot 6H_2O$, $Yb(NO_3)_3 \cdot 6H_2O$, $Tm(NO_3)_3 \cdot 6H_2O$, $La(NO_3)_3 \cdot 6H_2O$, $Ce(NO_3)_3 \cdot 6H_2O$, $Eu(NO_3)_3 \cdot 6H_2O$, $Gd(NO_3)_3 \cdot 6H_2O$, $Td(NO_3)_3 \cdot 6H_2O$ and $Er(NO_3)_3 \cdot 6H_2O$ were purchased from Shanghai Diyang Chemical Co., Ltd. NaF and MAA were purchased from Nanjing Chemical Reagent Co., Ltd. Polymerization inhibitor in MAA was removed by distillation before use. CDDP was obtained from Shandong Boyuan Chemical Co., Ltd. Other chemical reagents were analytical grade and used as received without further purification.

Preparation of rare-earth fluorides nanoparticles

$NaYF_4$:Yb^{3+}/Tm^{3+} nanoparticles were prepared by the following procedure. A certain amount of NaOH was dissolved by 5 mL of distilled water and 8 mL of absolute ethanol, into which were then added 2 mL of MAA and 1.2 mL of 0.5 M $Ln(NO_3)_3$ (Ln = 81.5% Y + 18% Yb + 0.5% Tm) aqueous solution. After stirring for 5 min, 4 mL of NaF aqueous solution (1 M) was added. After stirring for several minutes, the mixture was transferred into a 50 mL Teflon-lined stainless steel autoclave and heated at 120 °C for 8 h. After the autoclave was cooled to room temperature, white powders were collected by centrifugation, washed with distilled water three times and kept in distilled water. Other rare-earth doped fluorides were prepared when the amount of NaOH was 240 mg and the other reaction conditions were kept unchanged.

CDDP loading on $NaYF_4$:Yb^{3+}/Tm^{3+} nanoparticles

$NaYF_4$–CDDP composite was obtained by mixing 30 mg CDDP with 100 mg $NaYF_4$:Yb^{3+}/Tm^{3+} nanoparticles in 20 mL of distilled water under stirring at room temperature in dark for 24 h. The as-prepared $NaYF_4$–CDDP composite was centrifuged and washed with distilled water several times to remove the redundant CDDP. All the supernatants were collected and diluted in a volumetric flask. CDDP concentration in the supernatant was detected by atomic adsorption spectrum, and minusing was used to get the drug loading content.

In vitro CDDP release

The releases of CDDP from $NaYF_4$–CDDP composite in phosphate-buffered saline (PBS) (pH = 7.4) and HAc–NaAc buffer (pH = 5.5) at 37 °C were evaluated by the dialysis method as reported.[38] $NaYF_4$–CDDP composite (20 mg) was dispersed in PBS (pH = 7.4, 5 mL) and HAc–NaAc buffer (pH = 5.5, 5 mL), and then the suspension was transferred into a dialysis bag (3000 Da) and dialyzed in PBS (pH = 7.4, 200 mL) and HAc–NaAc buffer (pH = 5.5, 200 mL) at 37 °C respectively. CDDP in the external solution was sampled at defined time and measured by using inductively coupled plasma mass spectrometry (ICP-MS).

In vitro cytotoxicity assay

The cytotoxicities of $NaYF_4$–CDDP, $NaYF_4$:Yb^{3+}/Tm^{3+} nanoparticles and CDDP were measured by the 3-(4,5-dimethylthiazol-2-yl)-2,5-diphenyltetrazolium bromide (MTT) assay against human cervical cancer cell line (HeLa cells) and human breast adenocarcinoma cell line (MCF-7 cells). HeLa cells and MCF-7 cells were seeded in 96-well plates at 3000 cells per well in Dulbecco's modified Eagle's medium and incubated

at 37 °C with 5% CO_2 for 12 h. Then the cells were treated with fresh medium containing gradient concentrations (in terms of CDDP) of $NaYF_4$–CDDP, $NaYF_4$:Yb^{3+}/Tm^{3+} nanoparticles and CDDP, respectively. The cells were subsequently incubated for 24 or 48 h. Thereafter, 20 μL of MTT (final concentration: 5 mg mL^{-1}) was added to these wells, and the mixture was incubated for another 4 h. After the culture medium was replaced with 150 mL of dimethyl sulfoxide, the absorbance of MTT formazan was monitored at 570 nm using an automatic enzyme-linked immunosorbent assay plate reader. Cytotoxicity was expressed as the percentage of cell viability, and the cell viability was calculated based on the data of four replicate tests. The viability is expressed as mean ± S.D.

Cellular uptake and cell imaging

Glass coverslip (18 mm × 18 mm) was placed in each well of a 6-well plate. HeLa cells were planted on these glass coverslips in 6-well plate at 2.0 × 10^5 cells per well overnight for attachment. Then the cells were washed with PBS twice, and incubated in 1 mL of culture medium containing 400 μg $NaYF_4$–CDDP or $NaYF_4$:Yb^{3+}/Tm^{3+} nanoparticles for definite time at 37 °C in 5% CO_2. After the glass coverslips were washed with PBS carefully three times, the cells were fixed using 4% paraformaldehyde solution. After being rinsed with PBS three times, the glass coverslips were transferred onto glass slides with glycerol on them. Upconversion luminescence imaging was performed using a modified Zeiss optical microscope, with a CW NIR laser at λ_{ex} = 980 nm as an additional excitation source.

Characterization

X-ray powder diffractions (XRD) of the as-prepared products were measured by a Bruker D8 Advance instrument with Cu Kα radiation (λ = 0.15406 nm) at a scanning rate of 0.2° s^{-1} with 2θ range from 10 to 80°. Transmission electron microscopy (TEM) images were obtained using JEM-1011 instrument microscope at an acceleration voltage of 100 kV. Infrared (IR) spectroscopy was carried out by using Bruker IR vector22 infrared spectrometer in the wavenumber range from 4000 to 400 cm^{-1}. Degree of polymerization was detected on LCQ Fleet electrospray ionization mass spectrometer (ESI-MS) with negative ion mode. Thermogravimetric analysis (TGA) was analyzed using Pyris 1 thermo-analytical instrument under nitrogen flow (20 mL min^{-1}) at a heating rate of 10 K min^{-1}. X-ray photoelectron spectroscopy (XPS) was conducted on Thermo Scientific K-Alpha equipment, and the binding energy was referred to as the C1s photoelectron peak. Concentration of Pt was measured by ICP-MS using a standard Plasma-Quad II instrument, and each sample was repeated three times. Upconversion luminescent spectra were captured in the wave range of 300 to 550 nm on a Zolix luminescence spectrometer equipped with a 980 nm laser device at the power of 1 W. Upconversion luminescence images were acquired on the Zeiss primo star optical microscope, with a CW NIR laser at λ_{ex} = 980 nm as an additional excitation source, and with a Samsung pad as an image acquisition device.

Results and discussion

XRD was used to investigate the crystal structure of the as-prepared nanoparticles. The product was pure cubic phase $NaYF_4$ (JCPDS no. 77-2042) when no NaOH was added to the reaction system (Fig. 1a). Then diffraction peaks (Fig. 1b) indexed to hexagonal phase $NaYF_4$ (JCPDS no. 16-0334) appeared in the presence of 240 mg NaOH, which increased with rising amount of NaOH (Fig. 1c–e). Since a slow crystallization process might be preferable for achieving hexagonal phase $NaYF_4$,[28,39] raising the dosage of NaOH increased the amount of OH^- which decreased the effective concentration of Y^{3+} cations after binding them, and further reduced the crystallization velocity of $NaYF_4$. Therefore, hexagonal phase $NaYF_4$ increased when more NaOH was used.

Morphologies of the as-prepared nanoparticles were also influenced by the amount of NaOH. Fig. 2 shows the TEM images of corresponding products. The as-obtained products were branched (Fig. 2a) when no NaOH was used. When the dosage of NaOH was raised to 240 mg, the as-prepared products were nanoparticles with an average diameter lower than 100 nm (73 ± 35.4 nm). Afterwards, large nanoparticles (Fig. 2c–e) appeared with increasing amount of NaOH. Notably, some small nanoparticles were hollow (Fig. 2d and e), which may be attributed to Ostwald ripening.[1,40]

IR spectrum was introduced to identify the capping ligands on the surface of these as-prepared nanoparticles (Fig. 3). As shown in Fig. 3a–c, the peaks at 1556 and 1484 cm^{-1} correspond to the asymmetric and symmetric stretching vibrations of bound carboxyl groups respectively, suggesting the binding of carboxyl on the surface of these $NaYF_4$:Yb^{3+}/Tm^{3+} nanoparticles.[28] The peaks at 2996 and 2933 cm^{-1} represent the asymmetric and symmetric stretching vibrations of C–H bond respectively. The strong band at 1714 cm^{-1} can be assigned to the C=O asymmetric vibration of free carboxyl groups that improve the hydrophilicity of as-prepared $NaYF_4$:Yb^{3+}/Tm^{3+} nanoparticles.[28]

Since the carboxyl of MAA can bind rare-earth ion on the surface of $NaYF_4$:Yb^{3+}/Tm^{3+} nanoparticles, free carboxyl groups

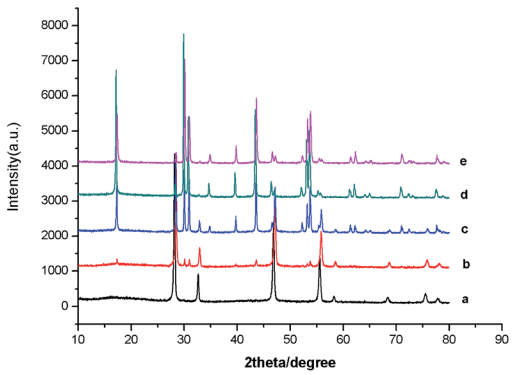

Fig. 1 XRD patterns of $NaYF_4$:Yb^{3+}/Tm^{3+} nanoparticles prepared at 120 °C for 8 h with different amounts of NaOH (a) 0 mg, (b) 240 mg, (c) 480 mg, (d) 720 mg and (e) 960 mg.

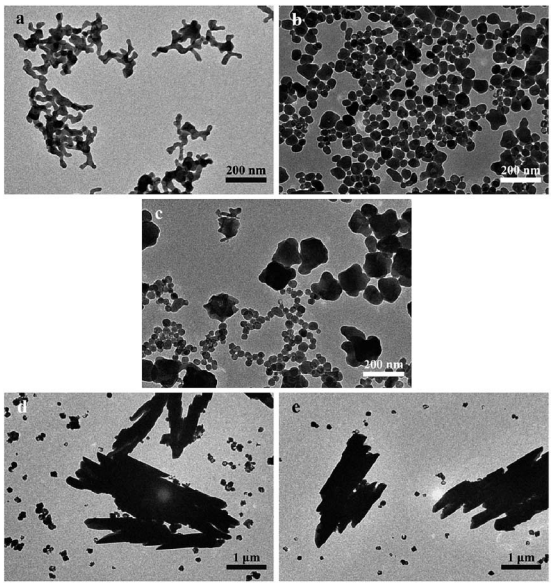

Fig. 2 TEM images of $NaYF_4$:Yb^{3+}/Tm^{3+} nanoparticles prepared with different amounts of NaOH (a) 0 mg, (b) 240 mg, (c) 480 mg, (d) 720 mg and (e) 960 mg.

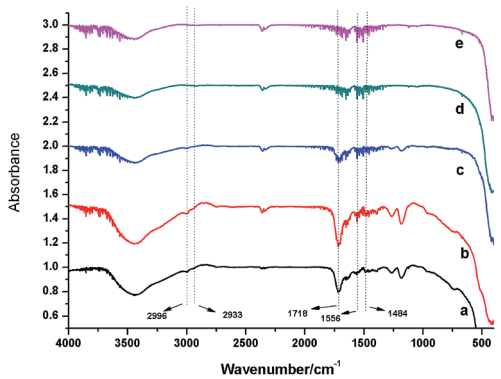

Fig. 3 IR spectra of $NaYF_4$:Yb^{3+}/Tm^{3+} nanoparticles prepared with different amounts of NaOH (a) 0 mg, (b) 240 mg, (c) 480 mg, (d) 720 mg and (e) 960 mg.

detected by IR spectra suggest the polymerization of MAA during hydrothermal process. Solute in the supernatant of hydrothermal reaction was detected by ESI-MS (Fig. S1†). MAA monomers polymerized during hydrothermal process, as compared with ESI-MS of the raw material (Fig. S2†). The degree of polymerization in the supernatant decreased when more NaOH was used, indicating that polymerization was favored under acidic conditions (Fig. S1a and b†). Control experiments with or without rare-earth ions demonstrated that rare-earth ions scarcely influenced the degree of polymerization (Fig. S3†). Thus, pH value was the key factor that influenced the polymerization degree of PMAA. Electrostatic effects varied due to the ionization degree of MAA which was elevated by adding NaOH, thereby strengthening the electrostatic repulsion between MAA monomer and the polymer chain and reducing the rate of polymerization.[41] As a result, the degree of polymerization was low at high pH value. Fig. 3d and e show that few ligands are capped on the surface of as-obtained products, although MAA polymerized with 720 and 960 mg NaOH (Fig. S1d and e†). When excessive NaOH was used during synthesis, abundant OH^- anions bound rare-earth cations instead of PMAA due to the low solubility constant of yttrium hydroxide (8×10^{-23}), thus sharply decreasing the amount of capping polymers. As no ligands were coated onto the surface of as-prepared $NaYF_4$:Yb^{3+}/Tm^{3+} nanoparticles, the grains grew in order to reduce the surface energy (Fig. 2d and e).

TGA was introduced to analyze the amount of capped ligands on the surface of as-obtained $NaYF_4$:Yb^{3+}/Tm^{3+} nanoparticles. The weight loss of $NaYF_4$:Yb^{3+}/Tm^{3+} nanoparticles was over 10% (Fig. 4a) and was less than 1% (Fig. 4e) without and with 960 mg NaOH respectively. The weight loss increased with decreasing NaOH amount. On one hand, the degree of polymerization was high in acidic condition; on the other hand, fewer OH^- anions were conducive to ligand bonding on the surface of these materials as mentioned above.

Other rare-earth doped fluorides were prepared when the amount of NaOH was 240 mg and the other reaction conditions were kept unchanged. As shown in Fig. 5, XRD patterns indicate that heavier rare-earth ions, such as Er^{3+}, Tm^{3+}, Yb^{3+}, tend to form cubic $NaErF_4$ (JCPDS no. 77-2041), $NaTmF_4$,[42] $NaYbF_4$ (JCPDS no. 77-2043) respectively, accompanied by slight hexagonal phase. Meanwhile, the cubic phase products increased with decreasing rare-earth ions radius. For rare-earth ions like Eu^{3+}, Gd^{3+} and Tb^{3+}, due to the increased dipole polarizability, the electron clouds of rare-earth ions tended to distort, and were thus prone to forming hexagonal $NaLnF_4$ ($NaEuF_4$ JCPDS no. 28-1085, $NaGdF_4$ JCPDS no. 27-0699, $NaTbF_4$ JCPDS no. 27-0809, Fig. 5c–e).[43] LnF_3 with hexagonal phase structures formed when the doped ions were lighter rare-earth ions such as La^{3+} and Ce^{3+} (LaF_3 JCPDS no. 32-0483, CeF_3 JCPDS no. 08-0045), because Na^+ cations hardly settled into the lattice of LnF_3 owing to the large radii of rare-earth ions.[44,45] ESI-MS of the solute in supernatant (Fig. S4†) reveals the polymerization of MAA. IR spectra (Fig. S5†) confirm these products were capped by carboxyl group. As other rare-earth compound

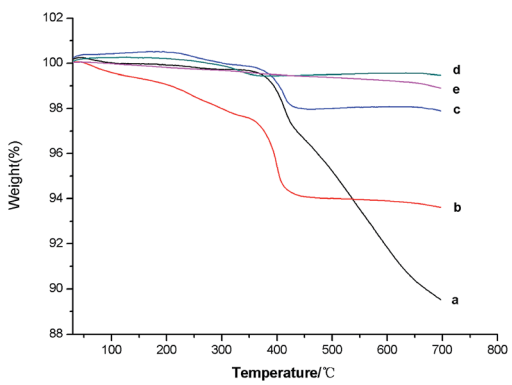

Fig. 4 TGA curves of $NaYF_4$:Yb^{3+}/Tm^{3+} nanoparticles prepared with different amounts of NaOH (a) 0 mg, (b) 240 mg, (c) 480 mg, (d) 720 mg and (e) 960 mg.

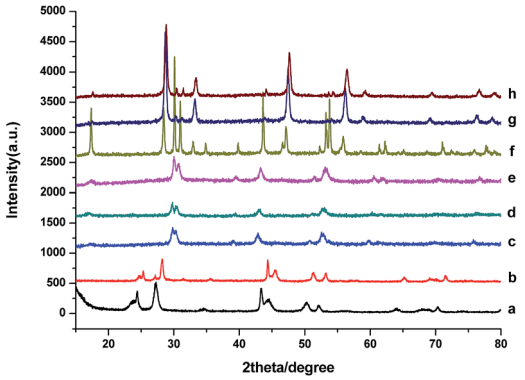

Fig. 5 XRD patterns of products prepared in the presence of 240 mg NaOH (a) LaF_3, (b) CeF_3, (c) $NaEuF_4$, (d) $NaGdF_4$, (e) $NaTbF_4$, (f) $NaErF_4$, (g) $NaTmF_4$, (h) $NaYbF_4$.

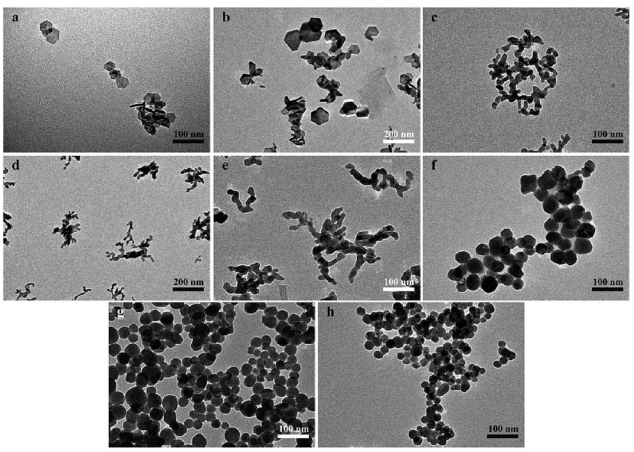

Fig. 6 TEM images of products prepared in the presence of 240 mg NaOH (a) LaF_3, (b) CeF_3, (c) $NaEuF_4$, (d) $NaGdF_4$, (e) $NaTbF_4$, (f) $NaErF_4$, (g) $NaTmF_4$, (h) $NaYbF_4$.

such as hydroxides and phosphates, morphologies of as-prepared rare-earth fluoride nanoparticles were also influenced by the ionic radii.[46] Fig. 6 shows the morphologies of the as-prepared products. LaF_3 and CeF_3 are hexagonal sheets, as shown in Fig. 6a and b. The products of $NaLnF_4$ were branched when the rare-earth ions were Eu^{3+}, Gd^{3+} and Tb^{3+} (Fig. 6c–e). Fig. 6f–h show the TEM images of $NaErF_4$, $NaTmF_4$ and $NaYbF_4$, exhibiting nanospheres all with small sizes.

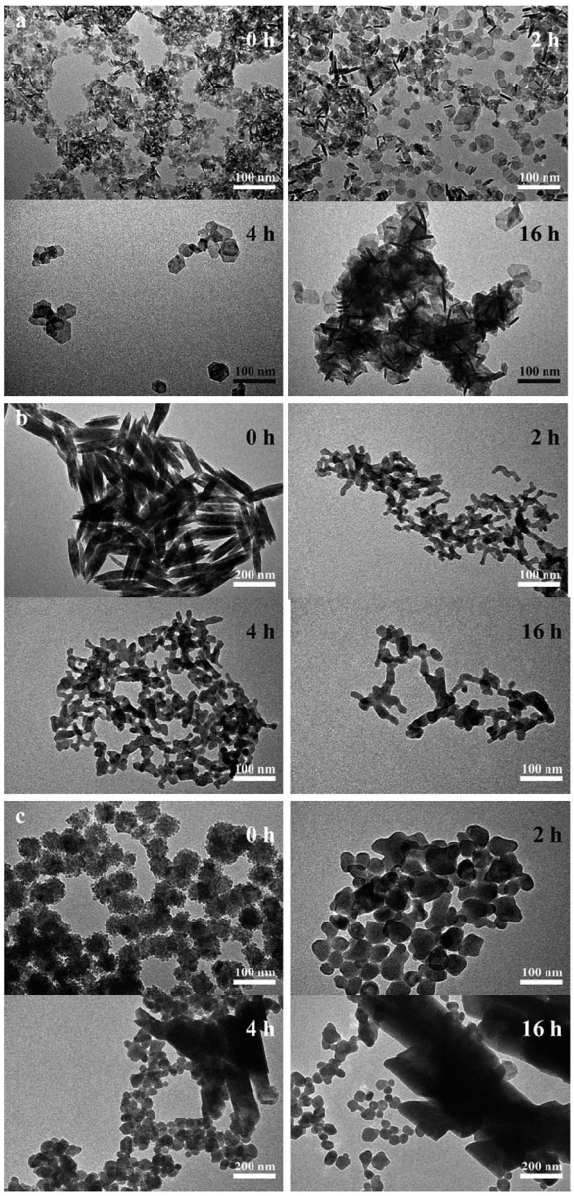

Fig. 8 TEM images of products prepared in the presence of 240 mg NaOH for different times (a) LaF_3, (b) $NaGdF_4$, (c) $NaYF_4$.

According to the structure and morphology, these products are divided into three classes, hexagonal phase LnF_3 (Ln = La^{3+} and Ce^{3+}), hexagonal phase $NaLnF_4$ (Ln = Eu^{3+}, Gd^{3+}, Tb^{3+}) and

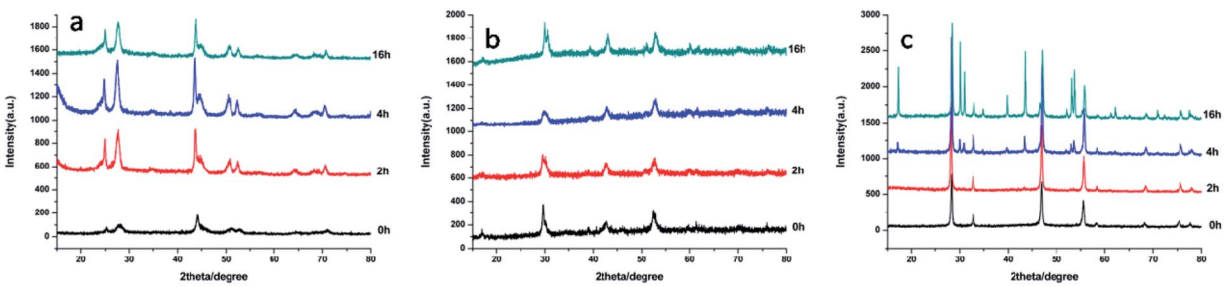

Fig. 7 XRD patterns of products prepared in the presence of 240 mg NaOH for different times (a) LaF_3, (b) $NaGdF_4$, (c) $NaYF_4$.

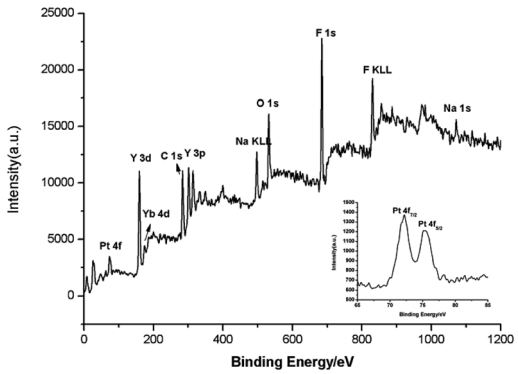

Fig. 9 XPS spectrum of $NaYF_4$–CDDP. Inset: enlarged spectrum of Pt4f.

cubic phase $NaLnF_4$ (Ln = Er^{3+}, Tm^{3+}, Yb^{3+}, Y^{3+}). LaF_3, $NaGdF_4$ and $NaYF_4$ were chosen to investigate the formation mechanism of these nano-materials. Hexagonal phase LaF_3 was obtained when the solvothermal time was 0 h, and the crystallinity degree increased as the reaction proceeded (Fig. 7a). Hexagonal phase $NaGdF_4$ formed at first and remained structurally unchanged with prolonged reaction time (Fig. 7b). As shown in Fig. 7c, pure cubic phase $NaYF_4$ was obtained when the solvothermal time was 0 h, which, however, began to transform to hexagonal phase at 4 h due to thermodynamic stability of the latter.[47,48]

TEM images show the morphology alteration of as-obtained products. Fig. 8a reveals that LaF_3 nanosheets appeared before solvothermal treatment, and these nanosheets grew to hexagonal sheets as the reaction time increased. As reported, the adsorption effect of ligands on different surface could lead to facets growing with different velocity.[1] In the case of LaF_3, PMAA might cap onto the upper and lower surface of nanosheets, and consequently reduced the energy and growing rate of these surfaces, prohibiting the thickness increase of LaF_3 nanosheets. The lack of PMAA adsorption on the other six surfaces drove the growth along the perpendicular direction of these surfaces, resulting in the radial enhancement of these nanosheets when prolonging reaction time.[1] The initial product of $NaGdF_4$ had loose structure comprising layers of nanosheets at the reaction temperature, which branched along with epitaxial growth following the no polymorphism branching mode (Fig. 8b).[42,49] The formation of multiarmed structure was also related to the adsorption of PMAA, as the bonding effect of ligand was different among crystal planes of $NaGdF_4$ nanoparticles. And the branched structure could further branched at the end of arms due to the same crystal phase of core and arms.[42] As shown in Fig. 8c, $NaYF_4$ seeds formed, aggregated into nano-clusters at the beginning of reaction, and further ripened into nanoparticles under solvothermal condition.

However, due to the thermodynamic unstability of cubic phase $NaYF_4$, small nanoparticles of $NaYF_4$ with cubic phase would transform into large particles which were hexagonal phase $NaYF_4$ according to XRD pattern through Ostwald-ripening (Fig. 7c). And large particles increased when prolonging reaction time.

$NaYF_4$:Yb^{3+}/Tm^{3+} nanoparticles were chosen to evaluate bioapplication of the as-prepared nano-materials. As surface free carboxyl groups enabled nanoparticles to further bind other molecules such as anticancer drugs, their amounts were obviously associated with weight loss of these as-obtained products, *i.e.* higher weight loss indicated larger amounts of free carboxyl groups. In general, abundant free carboxyl groups were required to load more drugs on these nanoparticles. Non-uniform, large nanoparticles were obtained when no NaOH was used in synthesis, although there were copious free carboxyl groups on the surface. Therefore, nanoparticles prepared with 240 mg NaOH were chosen as the drug carrier owing to suitable size (100 nm), which could be easily internalized into cells.[38,50]

The morphology and dispersibility of CDDP-loaded $NaYF_4$:Yb^{3+}/Tm^{3+} nanoparticles were observed by TEM. The morphology of $NaYF_4$–CDDP composite was the same as that of $NaYF_4$:Yb^{3+}/Tm^{3+} nanoparticles, and they were well dispersed without aggregation (Fig. S6†). As evidenced by the energy-dispersive X-ray spectrum (Fig. S7†) of $NaYF_4$–CDDP, Pt existed in the composite, suggesting that CDDP was successfully loaded onto the $NaYF_4$:Yb^{3+}/Tm^{3+} nanoparticles. Besides, Na, F, Y, Yb, Tm, C and O peaks could also be discerned. The loading manner of CDDP in $NaYF_4$:Yb^{3+}/Tm^{3+} nanoparticles were

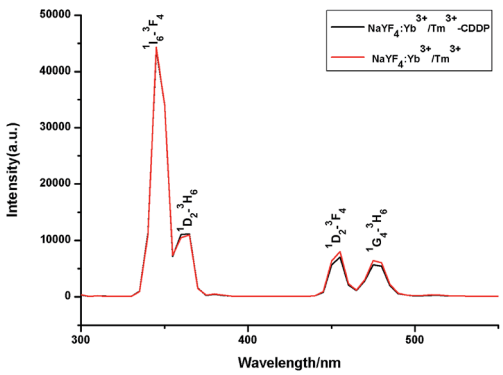

Fig. 10 Upconversion luminescence spectra of $NaYF_4$:Yb^{3+}/Tm^{3+} and $NaYF_4$–CDDP composite excited by a 980 nm CW laser.

Table 1 Pt contents (μg) in dialysis solution determined by ICP-MS at different times and pH values

	Dialysis time					
Solvent (pH)	3 h	6 h	12 h	24 h	48 h	72 h
HAc–NaAc (5.5)	9.04 ± 0.27	17.04 ± 0.20	23.42 ± 0.42	30.31 ± 0.37	40.92 ± 0.46	48.46 ± 0.71
PBS (7.4)	7.99 ± 0.06	15.29 ± 0.13	16.88 ± 0.27	18.31 ± 0.23	23.70 ± 0.32	26.24 ± 0.34

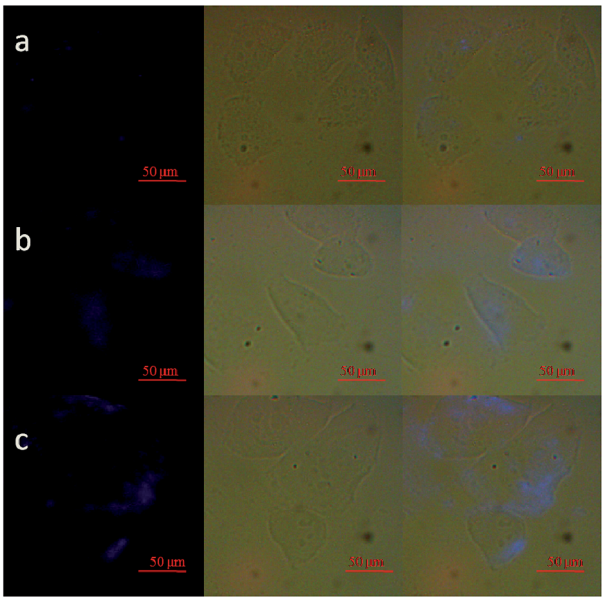

Fig. 11 Upconversion luminescence images of HeLa cells stained with 400 μg mL^{-1} $NaYF_4$–CDDP composite at 37 °C for (a) 3 h, (b) 12 h and (c) 24 h on the left, bright field images in the middle, and merged bright field and upconversion luminescence images on the right.

studied by XPS. As shown in Fig. 9, the photoelectron peaks of Y3d, Yb4d, C1s, O1s, F1s and Na1s are located at 158.5, 173.6, 287.9, 532.1, 684.4, and 1071.2 eV respectively. Moreover, the photoelectron peak corresponding to Pt4f was detected at 73 eV, which further demonstrated the formation of $NaYF_4$–CDDP composite. The close-up view of Pt4f region (inset of Fig. 9) exhibited two peaks at 72.4 and 75.7 eV for $Pt4f_{7/2}$ and $Pt4f_{5/2}$ respectively, *viz.*, the binding energy of Pt^{II} in Pt–O–C(O)–$NaYF_4$:Yb^{3+}/Tm^{3+} nanoparticles. Accordingly, CDDP was loaded through Pt–O bond.[51,52] The drug loading capacity was calculated by minusing method, and the mass percentage of CDDP in $NaYF_4$–CDDP composite was *ca.* 6.3%.

The release profile of CDDP from $NaYF_4$–CDDP composite was investigated in PBS (pH = 7.4) and HAc–HAc (pH = 5.5), respectively. Pt contents outside the dialysis bag are given in Table 1. CDDP was released sustainably from both buffers. Similar to a previous study,[38] the release of CDDP from $NaYF_4$–CDDP composite in HAc–NaAc (pH = 5.5) buffer was much faster than that in PBS (pH = 7.4), indicating that acidic environment, which resembled the microenvironment of tumor cells, benefited the release of CDDP from the nano-composite.[53]

When excited using a 980 nm CW laser, $NaYF_4$:Yb^{3+}/Tm^{3+} nanoparticles and $NaYF_4$–CDDP composite emitted bright blue lights. Fig. 10 shows the upconversion luminescence spectra of as-prepared $NaYF_4$:Yb^{3+}/Tm^{3+} nanoparticles and $NaYF_4$–CDDP composite excited at room temperature. There were two ultraviolet peaks and two visible peaks. Emission peaks at ~347, ~362, ~452 and ~477 nm correspond to the $^1I_6$–$^3F_4$, $^1D_2$–$^3H_6$, $^1D_2$–$^3F_4$ and $^1G_4$–$^3H_6$ transitions in Tm^{3+}, respectively.[54] Compared to $NaYF_4$:Yb^{3+}/Tm^{3+} nanoparticles, the upconversion luminescence intensity of $NaYF_4$–CDDP composite did not change evidently, *i.e.* the loading of CDDP barely influenced the luminescence property. As a result, uptake of $NaYF_4$–CDDP

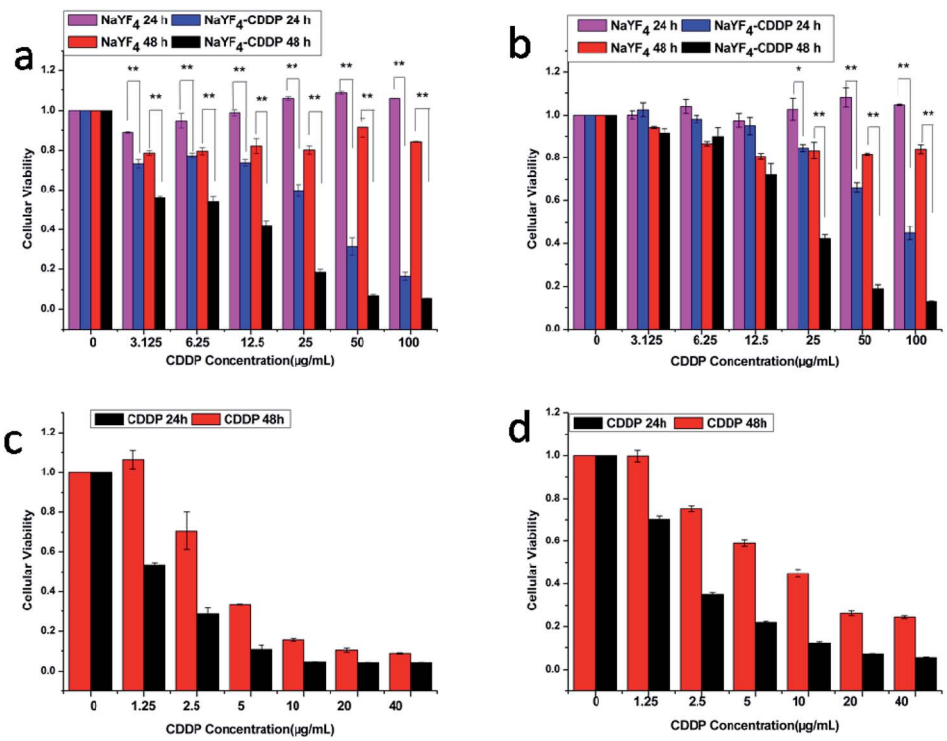

Fig. 12 Cytotoxicity of $NaYF_4$:Yb^{3+}/Tm^{3+} nanoparticles and $NaYF_4$–CDDP against HeLa (a) and MCF-7 (b) cancer cell lines at 24 and 48 h, respectively, with cytotoxicity of CDDP against HeLa (c) and MCF-7 (d) as the reference (*P < 0.05, **P < 0.01).

composite by cells could be monitored by detecting the upconversion luminescence of $NaYF_4$:Yb^{3+}/Tm^{3+} nanoparticles.

Nanoparticles can be internalized by cancer cells through endocytosis.[55] HeLa cells were used to monitor the cellular uptake process of $NaYF_4$–CDDP. HeLa cells incubated with the composite for different times were examined by microscopy equipped with a 980 nm CW laser. Only a few $NaYF_4$–CDDP composites were subjected to uptake by HeLa cells after being incubated for 3 h (Fig. 11a). The blue light was intensified when the incubation was prolonged to 12 h (Fig. 11b), indicating that more $NaYF_4$–CDDP was internalized and accumulated in the cytoplasm. Since intense blue light was detected in the cytoplasm after 24 h of incubation (Fig. 11c), much more composites were internalized into the cells with extended incubation time. In other words, the as-prepared $NaYF_4$–CDDP composite was internalized into cells slowly and time-dependently.

By using MTT assays, the antitumor capacity of $NaYF_4$–CDDP composite was tested against HeLa cells (Fig. 12a) and MCF-7 cells (Fig. 12b) with as-prepared $NaYF_4$:Yb^{3+}/Tm^{3+} nanoparticles as references. $NaYF_4$:Yb^{3+}/Tm^{3+} nanoparticles exhibited low cytotoxicity against cancer cells because over 80% of the cells survived even after incubation with high-concentration of them for 48 h. Compared with CDDP-free nanoparticles, $NaYF_4$–CDDP composite exerted more remarkable inhibitory effects on these cells. The half-maximal inhibitory concentrations (IC_{50}) of the composite against HeLa cells were 33.6 μg mL^{-1} and 8.36 μg mL^{-1} after 24 h and 48 h of incubation respectively, and they were 87.6 μg mL^{-1} and 21.7 μg mL^{-1} toward MCF-7 cells. The IC_{50} values of CDDP against HeLa cells were 5.12 μg mL^{-1} and 2.09 μg mL^{-1} at 24 h and 48 h, respectively, and they were 9.20 μg mL^{-1} and 2.31 μg mL^{-1} toward MCF-7 cells (Fig. 12c and d). The cytotoxicity of as-obtained composite was more time-dependent than that of CDDP, probably because the composite needed time to enter cells and released CDDP slowly due to the favorable releasing profile in the acid environment of cancer cells.[38,56]

The as-prepared $NaYF_4$:Yb^{3+}/Tm^{3+} nanoparticles, which were highly biocompatible and hydrophilic, were tested for possible application in cell imaging. HeLa cells were incubated with 400 μg mL^{-1} $NaYF_4$:Yb^{3+}/Tm^{3+} nanoparticles for 12 h or 24 h. Incubation for 12 h only gave dim blue light in the cells (Fig. S8a†), but the upconversion luminescence was enhanced at 24 h (Fig. S8b†). In other words, more $NaYF_4$:Yb^{3+}/Tm^{3+} nanoparticles entered the cells with extended incubation time. Accordingly, the as-produced $NaYF_4$:Yb^{3+}/Tm^{3+} nanoparticles were suitable for cell imaging *in vitro*.

Conclusions

In summary, we herein reported a facile method for preparation of carboxyl polymer-coated $NaYF_4$:Yb^{3+}/Tm^{3+} nanoparticles and other rare-earth doped fluorides nano-materials. The carboxyl group of $NaYF_4$:Yb^{3+}/Tm^{3+} nanoparticles produced by polymerization of MAA rendered them hydrophilic, and bound CDDP in the form of Pt–O bond. Cytotoxicity assay of $NaYF_4$–CDDP demonstrated that these as-prepared composites could deliver CDDP and kill cancer cells. $NaYF_4$:Yb^{3+}/Tm^{3+} nanoparticles were also successfully applied in upconversion luminescence imaging. Therefore, the as-prepared $NaYF_4$:Yb^{3+}/Tm^{3+} nanoparticles are feasibly applicable to simultaneous drug delivery and cell imaging.

Acknowledgements

This work is supported by the National Basic Research Program of China (2013CB922102) and the National Natural Science Foundation of China (21275072, 21201101 and 21475059).

Notes and references

1 Z. M. Chen, Z. R. Geng, M. L. Shi, Z. H. Liu and Z. L. Wang, *CrystEngComm*, 2009, **11**, 1591.
2 D. M. Yang, G. G. Li, X. J. Kang, Z. Y. Cheng, P. A. Ma, C. Peng, H. Z. Lian, C. X. Li and J. Lin, *Nanoscale*, 2012, **4**, 3450.
3 S. Heer, K. Kömpe, H. U. Güdel and M. Haase, *Adv. Mater.*, 2004, **16**, 2102.
4 F. Wang and X. G. Liu, *Chem. Soc. Rev.*, 2009, **38**, 976.
5 S. L. Smitha, K. M. Nissamudeen, D. Philip and K. G. Gopchandran, *Spectrochim. Acta, Part A*, 2008, **71**, 186.
6 Y. B. Song, S. J. Zhu and B. Yang, *RSC Adv.*, 2014, **4**, 27184.
7 L. Y. Chen, C. W. Wang, Z. Q. Yuan and H. T. Chang, *Anal. Chem.*, 2015, **87**, 216.
8 M. M. Madathil, C. Bhattacharya, Z. Q. Yu, R. Paul, M. J. Rishel and S. M. Hecht, *Biochemistry*, 2014, **53**, 6800.
9 K. Joo, Y. Fang, Y. Liu, L. Xiao, Z. Gu, A. Tai, C. L. Lee, Y. Tang and P. Wang, *ACS Nano*, 2011, **5**, 3523.
10 Z. Q. Yu, R. M. Schmaltz, T. C. Bozeman, R. Paul, M. J. Rishel, K. S. Tsosie and S. M. Hecht, *J. Am. Chem. Soc.*, 2013, **135**, 2883.
11 Z. G. Chen, H. L. Chen, H. Hu, M. X. Yu, F. Y. Li, Q. Zhang, Z. G. Zhou, T. Yi and C. H. Huang, *J. Am. Chem. Soc.*, 2008, **130**, 3023.
12 M. Nyk, R. Kumar, T. Y. Ohulchanskyy, E. J. Bergey and P. N. Prasad, *Nano Lett.*, 2008, **8**, 3834.
13 M. Haase and H. Schäfer, *Angew. Chem., Int. Ed.*, 2011, **50**, 5808.
14 G. Chen, T. Y. Ohulchanskyy, S. Liu, W. C. Law, F. Wu, M. T. Swihart, H. Ågren and P. N. Prasad, *ACS Nano*, 2012, **6**, 2969.
15 H. H. Gorris, R. Ali, S. M. Saleh and O. S. Wolfbeis, *Adv. Mater.*, 2011, **23**, 1652.
16 F. Han, Z. P. Guan, T. S. Tan and Q. H. Xu, *ACS Appl. Mater. Interfaces*, 2012, **4**, 4746.
17 G. S. Yi and G. M. Chow, *Adv. Funct. Mater.*, 2006, **16**, 2324.
18 C. B. Dong, Z. J. Yan, J. Kokx, D. B. Chrisey and C. Z. Dinu, *Appl. Surf. Sci.*, 2012, **258**, 9218.
19 C. B. Dong, R. Eldawud, L. M. Sargent, M. L. Kashon, D. Lowry, Y. Rojanasakul and C. Z. Dinu, *Environ. Sci.*, 2014, **1**, 595.
20 L. Cheng, C. Wang, L. Z. Feng, K. Yang and Z. Liu, *Chem. Rev.*, 2014, **114**, 10869.
21 Q. X. Mu, G. B. Jiang, L. X. Chen, H. Y. Zhou, D. Fourches, A. Tropsha and B. Yan, *Chem. Rev.*, 2014, **114**, 7740.

22 L. Y. Wang and Y. D. Li, *Chem. Commun.*, 2006, 2557.
23 L. X. Xie, Y. Qin and H. Y. Chen, *Anal. Chem.*, 2013, **85**, 2617.
24 M. Wang, C. C. Mi, W. X. Wang, C. H. Liu, Y. F. Wu, Z. R. Xu, C. B. Mao and S. K. Xu, *ACS Nano*, 2009, **3**, 1580.
25 C. Wang, L. Cheng and Z. Liu, *Biomaterials*, 2011, **32**, 1110.
26 J. N. Liu, W. B. Bu, L. M. Pan, S. J. Zhang, F. Chen, L. P. Zhou, K. L. Zhao, W. J. Peng and J. L. Shi, *Biomaterials*, 2012, **33**, 7282.
27 R. Naccache, F. Vetrone, V. Mahalingam, L. A. Cuccia and J. A. Capobianco, *Chem. Mater.*, 2009, **21**, 717.
28 Z. Wang, C. H. Liu, L. J. Chang and Z. P. Li, *J. Mater. Chem.*, 2012, **22**, 12186.
29 L. Y. Wang, Y. Zhang and Y. Y. Zhu, *Nano Res.*, 2010, **3**, 317.
30 M. Wang, C. C. Mi, J. L. Liu, X. L. Wu, Y. X. Zhang, W. Hou, F. Li and S. K. Sun, *J. Alloys Compd.*, 2009, **485**, L24.
31 X. J. Wu, Q. B. Zhang, X. Wang, H. Yang and Y. M. Zhu, *Eur. J. Inorg. Chem.*, 2011, **13**, 2158.
32 F. Wang, D. Banerjee, Y. S. Liu, X. Y. Chen and X. G. Liu, *Analyst*, 2010, **135**, 1839.
33 J. Zhou, M. X. Yu, Y. Sun, X. Z. Zhang, X. J. Zhu, Z. H. Wu, D. M. Wu and F. Y. Li, *Biomaterials*, 2011, **32**, 1148.
34 G. S. Yi and G. M. Chow, *Chem. Mater.*, 2007, **19**, 341.
35 H. Xu, L. Cheng, C. Wang, X. X. Ma, Y. G. Li and Z. Liu, *Biomaterials*, 2011, **32**, 9364.
36 Y. L. Dai, P. A. Ma, Z. Y. Cheng, X. J. Kang, X. Zhang, Z. Y. Hou, C. X. Li, D. M. Yang, X. F. Zhai and J. Lin, *ACS Nano*, 2012, **6**, 3327.
37 L. Li, C. Liu, L. Y. Zhang, T. T. Wang, H. Yu, C. Q. Wang and Z. M. Su, *Nanoscale*, 2013, **5**, 2249.
38 J. Z. Wang, X. Y. Wang, Y. J. Song, J. Wang, C. L. Zhang, C. J. Chang, J. Yan, L. Qiu, M. M. Wu and Z. J. Guo, *Chem. Sci.*, 2013, **4**, 2605.
39 Y. Wei, F. Q. Lu, X. R. Zhang and D. P. Chen, *Chem. Mater.*, 2006, **18**, 5733.
40 X. W. Lou, Y. Wang, C. L. Yuan, J. Y. Lee and L. A. Archer, *Adv. Mater.*, 2006, **18**, 2325.
41 I. Rintoul and C. Wandrey, *Polymer*, 2005, **46**, 4525.
42 X. Liang, X. Wang, J. Zhuang, Q. Peng and Y. D. Li, *Inorg. Chem.*, 2007, **46**, 6050.
43 F. Wang, Y. Han, C. S. Lim, Y. H. Lu, J. Wang, J. Xu, H. Y. Chen, C. Zhang, M. H. Hong and X. G. Liu, *Nature*, 2010, **463**, 1061.
44 Z. Wang, C. H. Liu, Y. C. Wang and Z. P. Li, *J. Alloys Compd.*, 2011, **509**, 1964.
45 J. H. Zeng, Z. H. Li, J. Su, L. Y. Wang, R. X. Yan and Y. D. Li, *Nanotechnology*, 2006, **17**, 3549.
46 S. L. Gai, G. X. Yang, X. B. Li, C. X. Li, Y. L. Dai, F. He and P. P. Yang, *Dalton Trans.*, 2012, **41**, 11716.
47 R. E. Thoma, H. Insley and G. M. Hebert, *Inorg. Chem.*, 1966, **5**, 1222.
48 H. X. Mai, Y. W. Zhang, R. Si, Z. G. Yan, L. D. Sun, L. P. You and C. H. Yan, *J. Am. Chem. Soc.*, 2006, **128**, 6426.
49 S. Chen, Z. L. Wang, J. Ballto, S. H. Foulger and D. L. Carroll, *J. Am. Chem. Soc.*, 2003, **125**, 16186.
50 H. Kato, *Nat. Nanotechnol.*, 2011, **6**, 139.
51 R. M. Xing, X. Y. Wang, C. L. Zhang, J. Z. Wang, Y. M. Zhang, Y. Song and Z. J. Guo, *J. Mater. Chem.*, 2011, **21**, 11142.
52 T. C. Deivaraj, W. X. Chen and J. Y. Lee, *J. Mater. Chem.*, 2003, **13**, 2555.
53 I. F. Tannock and D. Rotin, *Cancer Res.*, 1989, **49**, 4373.
54 F. Shi, J. S. Wang, X. S. Zhai, D. Zhao and W. P. Qin, *CrystEngComm*, 2011, **13**, 3782.
55 M. N. Moore, *Environ. Int.*, 2006, **32**, 967.
56 R. Haag and F. Kratz, *Angew. Chem., Int. Ed.*, 2006, **45**, 1198.